RSC Advances

PAPER

View Article Online
View Journal | View Issue

Cite this: *RSC Adv.*, 2023, **13**, 4168

A novel hierarchical book-like structured sodium manganite for high-stable sodium-ion batteries†

Yue Zhang, Hang Wang, Yakun Tang, Yudai Huang and Dianzeng Jia *

Received 2nd September 2022
Accepted 5th January 2023

DOI: 10.1039/d2ra05524d

rsc.li/rsc-advances

As one of the most promising cathodes for rechargeable sodium-ion batteries (SIBs), Layered transition metal oxides with high energy density show poor cycling stability. Judicious design/construction of electrode materials plays a very important role in cycling performance. Herein, a P2-$Na_{0.7}MnO_{2.05}$ cathode material with hierarchical book-like morphology combining exposed (100) active crystal facets is synthesized by hydrothermal method. Owing to the superiority of the unique hierarchical structure, the electrode delivers a high reversible capacity of 163 mA h g^{-1} at 0.2C and remarkable high-rate cyclability (88.8% capacity retention after 300 cycles at 10C). Its unique oriented stacking nanosheet constructed hierarchical book-like structure is the origin of the high electrochemical performance, which is able to shorten the diffusion distances of Na^+ and electrons, and a certain gap between the nanosheets can also relieve the stress and strain of volume generated during the cycle. In addition, the exposed (100) active crystal facets can provide more channels for the efficient transfer of Na^+. Our strategy reported here opens a door to the development of high-stable oxide cathodes for high energy density SIBs.

Introduction

With the deterioration of the natural environment, the environmental pollution associated with fossil fuels should be avoided as much as possible.[1–3] Recently, large-scale energy storage technology has received significant attention to make full use of clean energy such as wind, wave and solar.[4,5] Therefore, it is very important to seek a new type of secondary battery system with low cost, high safety and long cycle life for the application of large-scale energy storage equipment.[6–8] Because of the abundance and wide distribution of sodium resources, SIBs have become the primary choice for large-scale energy storage.[9–13] However, compared with lithium-ion batteries (LIBs), SIBs generally have a lower energy density due to the heavier and less reductive nature of sodium ions than lithium ions. To achieve high-energy SIBs, much attention has been focused on finding suitable cathode materials.[14–17]

Among various cathode materials, layered transition metal oxides are considered to be one of the most potential materials because of their high energy density and low cost.[18–21] In particular, layered sodium manganese oxides (Na_xMnO_{2+y}, y = 0.05–0.25) have attracted extensive attention due to their high theoretical capacity (243 mA h g^{-1}), low cost, and low toxicity.[22] However, the sluggish kinetics and frequent multiple phase transformations induced continuous volume expansion and contraction result in poor rate performance and deteriorated long cycle stability.[23] Recently, Zhang *et al.* synthesised a $AlPO_4$-coated P2-type hexagonal $Na_{0.7}MnO_{2.05}$ cathode material and enabled the capacity to increase from 93.8 to 104.0 mA h g^{-1}.[24] Lu *et al.* prepared polypyrrole-coated $Na_{0.7}MnO_{2.05}$ cathode material, delivering a reversible capacity up to 165.1 mA h g^{-1} at 100 mA g^{-1}.[22] Wang *et al.* designed a dual-ion co-doping strategy (Li and Cu) to activate the anion redox reaction in P2-$Na_{0.72}MnO_2$ cathode, exhibiting a stable cycling stability with a capacity retention of 80.1% after 150 cycles at 100 mA g^{-1}.[25] Although coating or doping can improve the electrochemical performance of sodium manganite, it is rare to get the reported results of ultralong cycling performances at high current densities (above 2000 mA g^{-1}, 10C).

Reasonable structure design can effectively enhance rate performance and alleviate capacity fading. For example, surfaces with high exposure ratio of (100) active crystal facets can provide more efficient diffusion channel for fast transfer of Na^+, which is beneficial for the improvement in rate capability.[26] Two-dimension (2D) nanosheets have attracted a lot of attention in fast Na^+ storage due to its ultrathin layered structure and infinite planar length, which not only provide short Na^+ transport pathway, but also facilitate the access of electrolyte ions.[27] However, disordered stacking of nanosheets will inevitably lead to lower volumetric energy and space transport barriers. An ideal structure model like book that the nanosheets are layered with orientation, in this way, high energy density can be ensured, and there is a certain gap between the nanosheets,

State Key Laboratory of Chemistry and Utilization of Carbon Based Energy Resources, College of Chemistry, Xinjiang University, Urumqi, 830017, Xinjiang, PR China. E-mail: jdz@xju.edu.cn

† Electronic supplementary information (ESI) available. See DOI: https://doi.org/10.1039/d2ra05524d

which can relieve the stress and strain caused by the constant phase transformation in the charging and discharging process. However, it remains a challenge to simultaneously achieve layered sodium manganese oxides with these beneficial structures.

Herein, P2-$Na_{0.7}MnO_{2.05}$ cathode material with hierarchical book-like morphology combining exposed (100) active crystal facets is successfully synthesized. The electrode exhibits outstanding electrochemical performances including excellent rate performance, and especially ultra-stable high-rate cyclability (88.8% capacity retention after 300 cycles at 10C). Thanks to its unique hierarchical book-like structure not only shorten the diffusion distances of ions/electrons and relieve the stress and strain of volume generated during the cycle, but also possesses high exposure ratio of (100) facets to achieve fast Na^+ storage.

Experimental section

Preparation of P2-$Na_{0.7}MnO_{2.05}$

All reagents were purchased from commercial suppliers, and used without further purification. First, 0.3 g polyacrylonitrile (PAN), 5 mmol $LiOH\cdot 2H_2O$ and 30 mL deionized water were transferred to a 100 mL hydrothermal kettle at 180 °C for 10 h to obtain modified polyacrylonitrile (MPAN). Then 5 mmol $Mn(AC)_2\cdot 2H_2O$ was added to 30 mL deionized water, and also transferred to 100 mL hydrothermal kettle after dissolving. After stirring for 30 min, the precipitate was heated at 180 °C for 16 h. The obtained precipitate was filtered and washed, and finally ground and mixed with anhydrous Na_2CO_3 with a certain molar ratio to $Mn(AC)_2\cdot 2H_2O$ of 0.35 : 1. The final product of P2-$Na_{0.7}MnO_{2.05}$ was obtained by calcination at 500 °C for 6 h and 850 °C for 8 h.

Material characterization

Morphologies and structure features of samples were studied by using field emission scanning electron microscope (FESEM JEOL JSM-7500F) and transmission electron microscope (TEM JEOL Tecnai G^2F-20). Phase compositions of samples were characterized by using X-ray diffraction (XRD, Bruker D8 advance with Cu Kα radiation).

Electrochemical characterization

2025 coin cells were adopted to measure electrochemical performances of all the samples, whereas sodium metal was used as the counter and reference electrodes. 75 wt% active materials, 15 wt% Ketjen black (type: EC-600JD) and 10 wt% poly (vinylidene fluoride) binder was dispersed in *N*-methyl-2-pyrrolidone to form slurries, which were casted on Al foil and dried at 110 °C overnight in vacuum. The typical loading of the active material on the Al foil was 1.5–2.5 mg cm^{-2} with about 1.5 μm. Cells were prepared in an argon-filled glove box, with glass fiber as the separator and $NaClO_4$ (1 M) in ethylene. Carbonate/propylene carbonate (1 : 1 v/v) as the electrolyte. Galvanostatic charge/discharge tests were carried out by using a Land (CT2001A China) between 1.5 and 4.5 V (*versus* Na/Na^+).

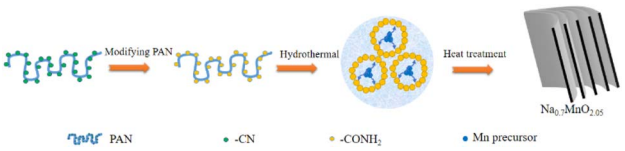

Fig. 1 Schematic synthesis process of hierarchical book-like P2-$Na_{0.7}MnO_{2.05}$.

Results and discussion

The schematic synthesis process of the hierarchical book-like P2-$Na_{0.7}MnO_{2.05}$ is displayed in Fig. 1 through a simple hydrothermal process and subsequent calcination. The morphology of P2-$Na_{0.7}MnO_{2.05}$ was examined by scanning electron microscopy (SEM). As shown in Fig. 2a, the sample displays a uniform flat micro-block structure. Its enlarged images of Fig. 2b and c show that the primary multiple-layer oriented stacking nanosheets assembling into secondary flat micro-block. This special hierarchical book-like structure could greatly enhance the electrochemical performance due to the short diffusion paths and flexible property induced by its primary multiple-layered structure. The crystal structure and phase purity of hierarchical book-like structured P2-$Na_{0.7}MnO_{2.05}$ was verified by XRD, as shown in Fig. 2d, all the XRD characteristic diffraction peaks can be matched well with layered P2-$Na_{0.7}MnO_{2.05}$ standard card (JCPDS card No. 27-0751).[22]

Further details about the distribution and morphology of the sample were confirmed by TEM images. As shown in Fig. 3a and b, the TEM images confirm again that the hierarchical book-like structure is made up of the directional stacking of ultrathin nanosheets. Its corresponding enlarged images shown in Fig. 3c, from this lattice-resolved high resolution TEM (HRTEM) image, the lattice fringe of crystal plane with spacing of 0.249 nm can be seen clearly, matching well with the lattice space of (100) facets of P2-$Na_{0.7}MnO_{2.05}$. The SAED image

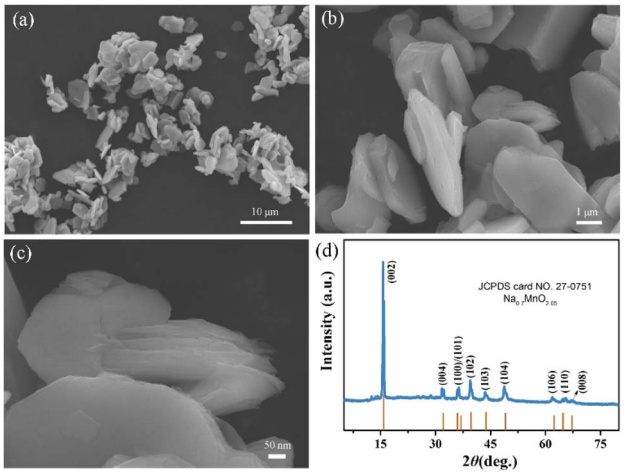

Fig. 2 (a–c) The SEM images of P2-$Na_{0.7}MnO_{2.05}$ with different magnification, (d) XRD diffraction pattern of P2-$Na_{0.7}MnO_{2.05}$.

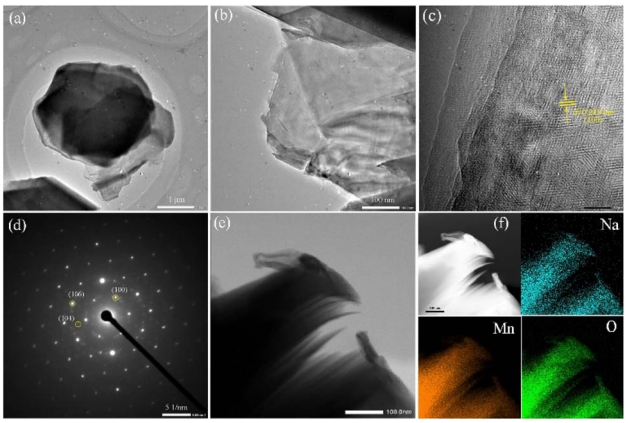

Fig. 3 The detailed structure analysis of P2-$Na_{0.7}MnO_{2.05}$: (a) TEM image and (b) a magnified image of (a); (c) HRTEM image; (d) SAED image; (e) HAADF image and (f) its corresponding EDS elementary mapping.

presented in Fig. 3d shows typical hexagonal diffraction spots of layered materials with diffraction spots corresponding to (100), (104) and (106) crystal planes, respectively, certifying again the existence of (100) crystal face. The hierarchical book-like structure with exposed (100) crystal facets could facilitate fast Na^+ inserting/extracting and ensure the stability of the cycle. The high-angle annular dark field (HAADF) image is displayed in Fig. 3e and f, demonstrating that Na, Mn and O elements are uniformly distributed throughout the hierarchical book-like structure.

Fig. 4 shows the electrochemical performance of P2-$Na_{0.7}MnO_{2.05}$ tested in Na half cells between 1.5 and 4.5 V (1C = 200 mA g^{-1}). The cyclic voltammetry (CV) curves of P2-$Na_{0.7}MnO_{2.05}$ electrode for the initial three cycles at a sweep rate of 0.1 mV s^{-1} is provided (Fig. 4a), showing two typical redox peaks pairs of 2.3 V/2.4 V and 4.25 V/4.1 V, which are similar to the reported Mn-based cathode materials of sodium ion batteries.[28] The peak pair 2.3 V/2.4 V are related to Mn^{4+}/Mn^{3+} and the high voltage peak pair 4.25 V/4.1 V can be attributed to the transition of P2 to O3 phase.[22,29] The other sharp and broad peaks are assigned to the two-phase transition and single-phase evolution during Na^+ inserting/extracting process.[30] Fig. 4b displays the cycling performance of the P2-$Na_{0.7}MnO_{2.05}$ at 1C, the initial discharge capacity of the electrode at 1C is 102 mA h g^{-1}. Moreover, the capacity retention is as high as 99.2% from the first to the 100 cycles and maintained almost 100% coulombic efficiency, highlighting the advantages of this unique hierarchical book-like structure in cycling performance. The galvanostatic charge/discharge profiles from first to 100 cycles at 1C are also provided in Fig. 4c. Notably, the galvanostatic charge/discharge profiles becomes smooth with the increase of cycle number, implying the enhancement of Na^+ transport kinetics.

To further demonstrate the advantage for the applications to high-rate SIBs, the rate performance of P2-$Na_{0.7}MnO_{2.05}$ is further tested from 0.2C to 5C (Fig. 4d), the P2-$Na_{0.7}MnO_{2.05}$ electrode delivers reversible capacities of 163, 131, 118, 106, and

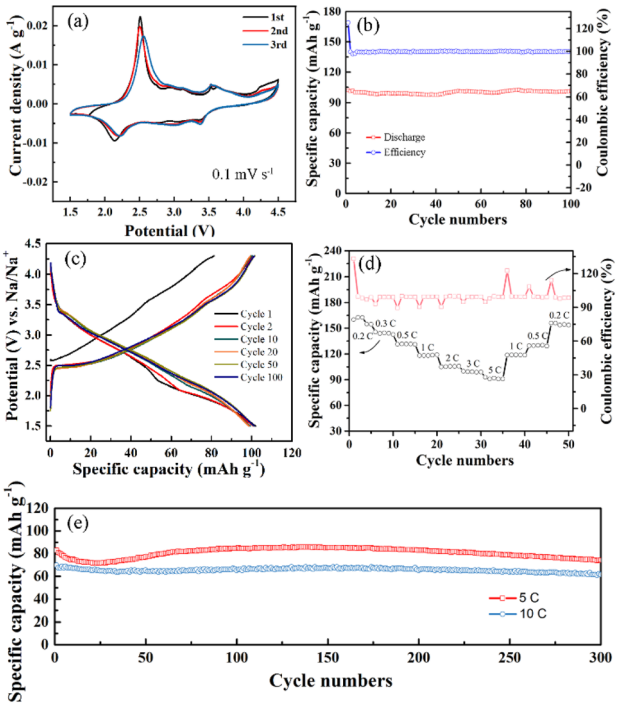

Fig. 4 Electrochemical performance of P2-$Na_{0.7}MnO_{2.05}$: (a) CV curves for the initial three cycles collected at a sweep rate of 0.1 mV s^{-1} (b) cycle performance and its corresponding galvanostatic charge/discharge profiles from first to 100 cycles at 1C (c); (d) rate performance; (e) cycle performance at 5C and 10C, respectively.

99 mA h g^{-1} at 0.2C, 0.5C, 1C, 2C, and 3C, respectively. Even at a high rate of 5C (1000 mA g^{-1}), a remarkably reversible capacity of 92 mA h g^{-1} could still be obtained. Compared with the capacity at 0.2C, the capacity retention at 5C is up to 57.5%. In addition, except for first cycle, the subsequent Coulomb efficiency at different rate is all close to 100%, indicating that the electrochemical reaction of the material is highly reversible. The cycling performance of P2-$Na_{0.7}MnO_{2.05}$ electrode at 5C is presented in Fig. 4e, a remarkably reversible capacity of 74.3 mA h g^{-1} could still be obtained after 300 cycles. The capacity retention from the first to the 300 cycles can be reached 89.3%. Due to the layered sodium manganese oxides often suffer from frequent multiple phase transformations upon cycling, it's difficult to obtain satisfactory long cycle stability at high current densities above 10C. In order to further highlight the superiority of this hierarchical book-like structure, the long cycling life performance at high rate of 10C is also presented in Fig. 4d. Remarkably, even at such high rate, the P2-$Na_{0.7}MnO_{2.05}$ electrode can still exhibit outstanding cycling stability. The discharge capacities of this electrode at the 50th, 100th and 200th cycles are all 66.5 mA h g^{-1}. Importantly, even after 300 cycles, the electrode can deliver a reversible capacity of 62 mA h g^{-1} as well, and the capacity retention is up to 88.8%. The cycling performances of our hierarchical book-like P2-$Na_{0.7}MnO_{2.05}$ is comparable to those similar cathode materials as shown in Table 1. SEM images of P2-$Na_{0.7}MnO_{2.05}$ sample after 100 cycles at 1C are provided and shown in Fig. S1,†

Table 1 A survey of electrochemical properties of similar cathode materials reported in the open literature

Typical materials	Current density	Cycle numbers	Remaining capacity (mA h g^{-1})	Ref.
$Na_{0.7}MnO_{2.05}$@$NaPO_3$	0.1 A g^{-1}	200	132.8	31
$Na_{0.7}MnO_{2.05}$@$AlPO_4$	1 A g^{-1}	100	96.0	24
$Na_{0.7}MnO_{2.05}$@PPy	0.1 A g^{-1}	100	142.6	22
O3-$NaNi_{0.5}Mn_{0.5}O_2$@P2-$Na_{2/3}MnO_2$	2C	200	108.2	32
	5C	400	83.6	
$Na_{2/3}Ni_{1/3}Mn_{2/3}O_2$@$Al_2O_3$	0.05C	200	77.43	33
Fast-cooled $Na_{0.7}MnO_2$	0.1C	50	146	34
$Na_{0.53}MnO_2$ nanorods	0.2C	50	91.3	35
$Na_{0.67}[Mn_{0.67}Ni_{0.21}Li_{0.06}Zn_{0.06}]O_2$	1C	500	103	36
$Na_{0.65}Mn_{0.75}Ni_{0.25}O_2$@$AlPO_4$	1C	200	82	37
$Na_{2/3}Ni_{1/3}Mn_{2/3}O_2$@ZnO	0.5C	200	70.7	38
Book-like P2-$Na_{0.7}MnO_{2.05}$	5C	300	74.3	This work
	10C	300	62	

oriented stacking nanosheets constructed hierarchical book-like structure is still retained after continuous charging/discharging processes, due to the certain gap between the nanosheets can relieve the stress and strain of volume generated during the cycle.

The electrochemical impedance spectroscopy (EIS) is performed to study the kinetics characteristics of the P2-$Na_{0.7}MnO_{2.05}$ at various cycling intervals at 1C from 0.01 Hz to 100 kHz. As shown in Fig. S2a,† the Nyquist plots consist of a semicircle in the high frequency range and sloping line in the low-frequency range, corresponding to the charge transfer resistance (R_{ct}) and Warburg impedance, respectively. Fig. S2b† shows the relationship between Z' and $\omega^{-0.5}$ of these two electrodes, displaying a linear characteristic for every curve.[39] The R_{ct} of P2-$Na_{0.7}MnO_{2.05}$ electrode before the charge–discharge tests is 341 Ω, while the R_{ct} of this electrode is 722, 609, 446, and 399 Ω after the 1st, 3rd, 10th and 20th cycle, respectively. An increase in the charge-transfer resistance would indicate capacity fading during the beginning of the cycle, due to the activation of electrode and the formation of a stable surface film, with further cycling, the resistance gradually drops and stabilizes at 399 Ω, suggesting a gradual stabilization of the cycling, which agrees well with the cycling test results. Importantly, the D of P2-$Na_{0.7}MnO_{2.05}$ electrode is greatly improved than that of P2-$Na_{0.7}MnO_{2.05}$ electrode without cycling from about 1.03×10^{-16} cm^2 s^{-1} to 2.81×10^{-16} cm^2 s^{-1}. The results imply that the charge transfer and the Na^+ diffusion are highly enhanced by the further cyclic activation.

The multiple-layer oriented stacking nanosheets constructed hierarchical book-like structure combining exposed (100) active crystal facets endow P2-$Na_{0.7}MnO_{2.05}$ cathode with excellent sodium storage behavior. First, the 2D stacked nanosheets acts as the electron and ion short transmission path, ensuring rapid electrochemical reaction. Besides, a certain gap between the multiple-layer oriented stacking nanosheets can relieve the stress and strain of volume, guaranteeing the excellent structure stability to withstand mechanical strain large induced by the frequent multiple phase transformations upon cycling process. Finally, the exposed (100) active crystal facets could provide more channels for the fast and efficient transfer of Na^+, contributing to the high rate capability.

Conclusions

In conclusion, P2-$Na_{0.7}MnO_{2.05}$ cathode material with hierarchical book-like morphology combining exposed (100) active crystal facets is successfully prepared. Multiple-layer oriented stacking nanosheets constructed hierarchical book-like structure not only shorten the diffusion distances of ions and electrons, but also relieve the mechanical strain large induced by the frequent multiple phase transformations upon cycling process. Meanwhile, the exposed (100) active crystal facets could provide more channels for the efficient transfer of Na^+. As a result, this P2-$Na_{0.7}MnO_{2.05}$ cathode exhibits excellent rate performance and superior cycling stability. Our strategy reported here opens a door to the development of high-stable oxide cathodes for high energy density SIBs.

Author contributions

All the authors have contributed to the results, analysis, and discussion, as well as manuscript preparation. They have approved the final version of the manuscript.

Conflicts of interest

There are no conflicts to declare.

Acknowledgements

This work was financially supported by the Natural Science Foundation of Xinjiang Uygur Autonomous Region of China (2021D01C090), the Xinjiang Tianshan Youth Doctoral Project (2019Q062), the National Natural Science Foundation of China (51902277), the Xinjiang Tianchi Doctoral Project (2020) and the Xinjiang University Doctoral Research Foundation (2019).

References

1 S.-L. Li and Q. Xu, *Energy Environ. Sci.*, 2013, **6**, 1656–1683.
2 M. Höök and X. Tang, *Energy Policy*, 2013, **52**, 797–809.
3 Q. Liu, Z. Hu, M. Chen, C. Zou, H. Jin, S. Wang, S.-L. Chou, Y. Liu and S.-X. Dou, *Adv. Funct. Mater.*, 2020, **30**, 1909530.
4 Y. Li, F. Wu, Y. Li, M. Liu, X. Feng, Y. Bai and C. Wu, *Chem. Soc. Rev.*, 2022, **51**, 4484–4536.
5 Z. Sun, Y. Zhao, Q. Ni, Y. Liu, C. Sun, J. Li and H. Jin, *Small*, 2022, **18**, 2200716.
6 Z. Yang, J. He, W.-H. Lai, J. Peng, X.-H. Liu, X.-X. He, X.-F. Guo, L. Li, Y. Qiao, J.-M. Ma, M. Wu and S.-L. Chou, *Angew. Chem., Int. Ed.*, 2021, **60**, 27086–27094.
7 Y. Liu, D. Wang, H. Li, P. Li, Y. Sun, Y. Liu, Y. Liu, B. Zhong, Z. Wu and X. Guo, *J. Mater. Chem. A*, 2022, **10**, 3869–3888.
8 S. Sun, Y. Chen, Q. Bai, Q. Huang, C. Liu, S. He, Y. Yang, Y. Wang and L. Guo, *J. Mater. Chem. A*, 2022, **10**, 11340–11353.
9 Z. Liang, H. Tu, K. Zhang, Z. Kong, M. Huang, D. Xu, S. Liu, Y. Wu and X. Hao, *Chem. Eng. J.*, 2022, **437**, 135421.
10 J. Liao, F. Zhang, Y. Lu, J. Ren, W. Wu, Z. Xu and X. Wu, *Chem. Eng. J.*, 2022, **437**, 135275.
11 Q. Xiao, Q. Song, K. Zheng, L. Zheng, Y. Zhu and Z. Chen, *Nano Energy*, 2022, **98**, 107326.
12 Y. Zhang, Z. Bi, Y. Liang, W. Zuo, G. Xu and M. Zhu, *Energy Storage Mater.*, 2022, **48**, 35–43.
13 H. Yu, M. Walsh and X. Liang, *ACS Appl. Mater. Interfaces*, 2021, **13**, 54884–54893.
14 J. Feng, S.-h. Luo, J. Wang, P. Li, S. Yan, J. Li, P.-q. Hou, Q. Wang, Y. Zhang and X. Liu, *ACS Sustainable Chem. Eng.*, 2022, **10**, 4994–5004.
15 Y. Zhang, J. Xun, K. Zhang, B. Zhang and H. Xu, *J. Mater. Chem. A*, 2022, **10**, 11163–11171.
16 F. Lu, J. Wang, S. Chang, L. He, M. Tang, Q. Wei, S. Mo and X. Kuang, *Carbon*, 2022, **196**, 562–572.
17 L. Zhang, J. Wang, G. Schuck, F. Xi, L. Du, M. Winter, G. Schumacher and J. Li, *Small Methods*, 2020, **4**, 2000422.
18 Z. Ma, Z. Zhao, H. Xu, J. Sun, X. He, Z. Lei, Z.-h. Liu, R. Jiang and Q. Li, *Small*, 2021, **17**, 2006259.
19 X.-G. Yuan, Y.-J. Guo, L. Gan, X.-A. Yang, W.-H. He, X.-S. Zhang, Y.-X. Yin, S. Xin, H.-R. Yao, Z. Huang and Y.-G. Guo, *Adv. Funct. Mater.*, 2022, **32**, 2111466.
20 Y. Pang, H. Li, S. Zhang, Q. Ma, P. Xiong, R. Wang, Y. Zhai, H. Li, H. Kang, Y. Liu, L. Zhang, L. Zhang, T. Zhou and C. Zhang, *J. Mater. Chem. A*, 2022, **10**, 1514–1521.
21 R. Luo, X. Hu, N. Zhang, L. Li, F. Wu and R. Chen, *Small*, 2022, **18**, 2105713.
22 D. Lu, Z. Yao, Y. Zhong, X. Wang, X. Xia, C. Gu, J. Wu and J. Tu, *ACS Appl. Mater. Interfaces*, 2019, **11**, 15630–15637.
23 Y. Xiao, P.-F. Wang, Y.-X. Yin, Y.-F. Zhu, Y.-B. Niu, X.-D. Zhang, J. Zhang, X. Yu, X.-D. Guo, B.-H. Zhong and Y.-G. Guo, *Adv. Mater.*, 2018, **30**, 1803765.
24 Y. Zhang, Y. Pei, W. Liu, S. Zhang, J. Xie, J. Xia, S. Nie, L. Liu and X. Wang, *Chem. Eng. J.*, 2020, **382**, 122697.
25 F. Wang, B. Peng, S. Y. Zeng, L. P. Zhao, X. L. Zhang, G. L. Wan, H. L. Zhang and G. Q. Zhang, *Adv. Funct. Mater.*, 2022, **32**, 2202665.
26 D. Su, C. Wang, H. J. Ahn and G. Wang, *Chem.–Eur. J.*, 2013, **19**, 10884–10889.
27 L. Gao, S. Chen, L. Zhang and X. Yang, *J. Power Sources*, 2018, **396**, 379–385.
28 J. Deng, W.-B. Luo, X. Lu, Q. Yao, Z. Wang, H.-K. Liu, H. Zhou and S.-X. Dou, *Adv. Energy Mater.*, 2018, **8**, 1701610.
29 C. Luo, A. Langrock, X. Fan, Y. Liang and C. Wang, *J. Mater. Chem. A*, 2017, **5**, 18214–18220.
30 D. H. Lee, J. Xu and Y. S. Meng, *Phys. Chem. Chem. Phys.*, 2013, **15**, 3304.
31 W. Li, Z. Yao, S. Zhang, X. Wang, X. Xia, C. Gu and J. Tu, *Chem. Eng. J.*, 2021, **421**, 127788.
32 X. Liang, T.-Y. Yu, H.-H. Ryu and Y.-K. Sun, *Energy Storage Mater.*, 2022, **47**, 515–525.
33 J. Alvarado, C. Ma, S. Wang, K. Nguyen, M. Kodur and Y. S. Meng, *ACS Appl. Mater. Interfaces*, 2017, **9**, 26518–26530.
34 M. A. Khan, D. Han, G. Lee, Y.-I. Kim and Y.-M. Kang, *J. Alloys Compd.*, 2019, **771**, 987–993.
35 J.-Y. Li, H.-Y. Lü, X.-H. Zhang, Y.-M. Xing, G. Wang, H.-Y. Guan and X.-L. Wu, *Chem. Eng. J.*, 2017, **316**, 499–505.
36 W. Li, Z. Yao, S. Zhang, X. Wang, X. Xia, C. Gu and J. Tu, *ACS Appl. Mater. Interfaces*, 2020, **12**, 41477–41484.
37 Y. Wang, K. Tang, X. Li, R. Yu, X. Zhang, Y. Huang, G. Chen, S. Jamil, S. Cao, X. Xie, Z. Luo and X. Wang, *Chem. Eng. J.*, 2019, **372**, 1066–1076.
38 Y. Yang, R. Dang, K. Wu, Q. Li, N. Li, X. Xiao and Z. Hu, *J. Phys. Chem. C*, 2020, **124**, 1780–1787.
39 W. He, C. J. Li, B. B. Zhao, X. D. Zhang, K. S. Hui and J. F. Zhu, *Chem. Eng. J.*, 2021, **403**, 126311.